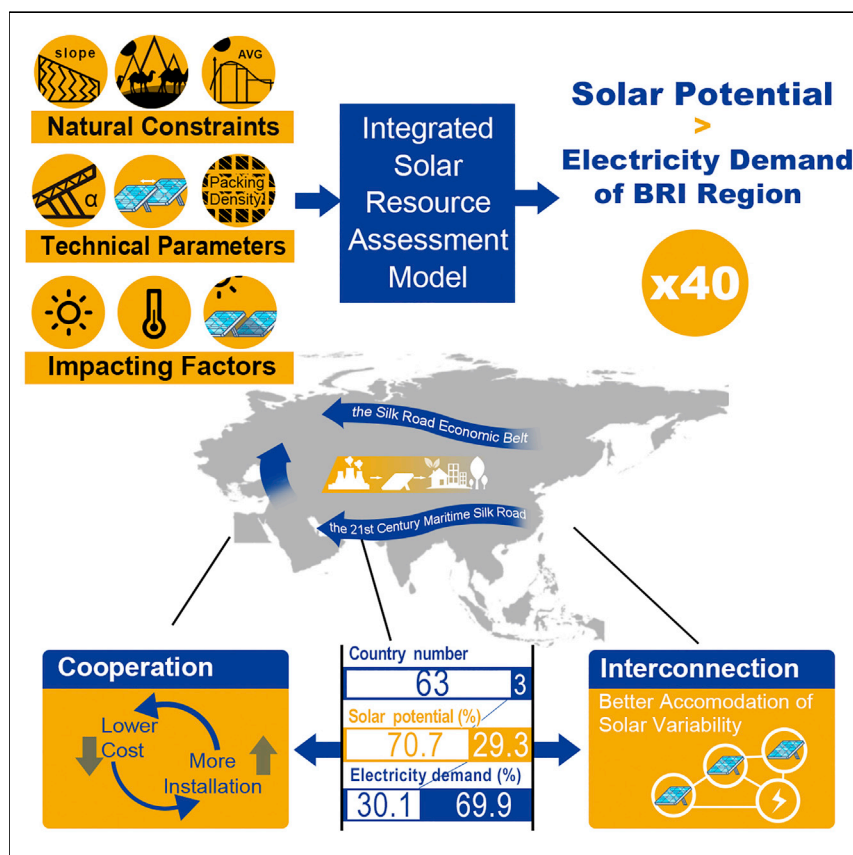


Article

# The Potential of Photovoltaics to Power the Belt and Road Initiative



Shi Chen, Xi Lu, Yufei Miao, ..., Kathryn G. Logan, Michael B. McElroy, Jiming Hao

xilu@tsinghua.edu.cn (X.L.)  
mbm@seas.harvard.edu (M.B.M.)

**HIGHLIGHTS**

Solar potential for BRI region is 41.3 times regional electricity demand of 2016.

Countries with 70.7% of the potential consume only 30.1% of regional electricity.

Mismatch between potential and demand highlights the merits of regional cooperation.

Regional grid interconnections facilitate higher penetration of variable solar power.

Carbon-intensive energy infrastructure in the BRI region has exacerbated prospects for climate change. An integrated model was developed to explore the potential of solar photovoltaics as a climate-friendly alternative to achieve the 2°C climate targets outlined in Paris. Results indicate that the solar photovoltaics potential in the BRI region is 41.3 times the regional electricity demand of 2016. The mismatch between technical potential and electricity consumption highlights the advantage of regional cooperation as well as investments in electric power grid interconnections.

Article

# The Potential of Photovoltaics to Power the Belt and Road Initiative

Shi Chen,<sup>1,8</sup> Xi Lu,<sup>1,8,9,\*</sup> Yufei Miao,<sup>2</sup> Yu Deng,<sup>3</sup> Chris P. Nielsen,<sup>4</sup> Noah Elbot,<sup>5</sup> Yuanchen Wang,<sup>1</sup> Kathryn G. Logan,<sup>6</sup> Michael B. McElroy,<sup>7,\*</sup> and Jiming Hao<sup>1</sup>

## SUMMARY

Construction of carbon-intensive energy infrastructure is well underway under the Belt & Road Initiative (BRI), challenging the global climate target. Regionally abundant solar power could provide an alternative for electricity generation. An integrative spatial model was developed to evaluate the technical potential of solar photovoltaic power. The influence of impacting factors was quantified systematically on an hourly basis. Results suggest that the electricity potential for the BRI region reaches 448.9 PWh annually, 41.3 times the regional demand for electricity in 2016. Tapping 3.7% of the potential through deploying 7.8 TW capacity could satisfy the regional electricity demand projected for 2030, requiring an investment of approximately 11.2 trillion 2017 USD and a commitment in land area of 88,426 km<sup>2</sup>, approximately 0.9% of China's total. Countries endowed with 70.7% of the overall potential consume only 30.1% of regional electricity. The imbalance underscores the advantage of regional cooperation and investments in interconnected grids.

## INTRODUCTION

The Belt and Road Initiative (BRI), launched by Chinese President Xi in 2013, aims to promote economic integration and development across the Eurasian Continent that could be both bilaterally and multilaterally beneficial. The BRI borrows the historical symbols of the ancient Silk Road, which originated in ancient China and connected Asia, Africa, and Europe through routes of commercial trade and cultural exchange. In the new usage, "Belt" refers to the overland "Silk Road Economic Belt" and "Road" to the 21<sup>st</sup>-century "Maritime Silk Road".<sup>1</sup> Although the BRI has become an open platform with 126 partner countries,<sup>2</sup> following the existing literature we selected a total of 66 countries geographically adjoining the Belt and Road as the territorial scope of the present analysis,<sup>3</sup> which emphasizes the likely concentrated infrastructure investment,<sup>4</sup> the rapidly growing regional electricity demand, and the potential advantages of regional energy collaboration (see [Tables S1 and S15](#)). In 2017, more than 30% of these BRI countries realized an annual gross domestic product (GDP) growth rate of more than 5% (see [Table S3](#)).<sup>5</sup> It is estimated that from 2015 to 2030, approximately 50% of the world's GDP growth could originate in the BRI region.<sup>6</sup> In the short run, the GDP per capita could result in a significant rise in carbon emissions and energy use in the BRI countries.<sup>7</sup> In 2016, about 1.1 billion people globally were without access to electricity, nearly 30% living in these BRI countries (see [Tables S2 and S5](#)).<sup>8–10</sup> Demand for electricity from the BRI countries is expected to undergo a significant increase in the future to fuel projected economic growth and to satisfy basic needs for electricity. Consequently, construction of energy infrastructure has been an essential element of cooperation among the BRI countries. The BRI investment was estimated at \$241.2 billion between 2014

## Context & Scale

The Belt and Road Initiative (BRI) highlights energy infrastructure construction to catalyze economic development, with fossil fuels predominating ongoing projects. If this trend continues, the build-up could result in an important source of CO<sub>2</sub>, threatening the limit in the rise of global average surface temperature of 2.0°C, or preferably 1.5°C, set in the Paris climate summit. Solar power could serve as an alternative to coal. Using high-resolution data, we evaluated on an hourly basis the potential of solar electricity over the BRI region with systematic consideration of the impacting factors. Results indicate that solar power could provide 448.9 PWh of electricity annually, 3.7% of which could meet the regional electricity demand projected for 2030. Regional grid interconnections could increase the overall efficiency of the system by utilizing the complementary effects in spatial and temporal variations of solar insolation and electricity demand across the region.

and 2017, more than 80% of which went to development of technologies using or facilitating the use of fossil fuel, including oil, gas, petrochemicals, and power generation.<sup>4</sup> An increasing global concern for climate mitigation arises if it continuously emphasizes fossil fuel-based combustion technologies. Potential further expansion of carbon-intensive power plants in this region would create a significant new source of carbon emissions and, even worse, once these plants are constructed, they would be expected to operate over multiple decades, adding CO<sub>2</sub> continuously to the atmosphere.

Solar power locally available in the BRI countries could provide an important life cycle environment-friendly alternative to replace, or at least mitigate, fossil-based power generation,<sup>11</sup> offering an opportunity to decouple future economic growth from increasing carbon emissions. The BRI region as defined in this study spans three continents (Europe, Asia and Africa), including the desert nations of West Asia, which are endowed with some of the most abundant solar resources in the world.<sup>12</sup> Approximately 53% of the land area in the BRI region has annual solar radiation intensities higher than 1400 kWh/(m<sup>2</sup>·a), taken as the lower limit for economically viable development of solar projects in China.<sup>13</sup> The global installed capacity for solar photovoltaics (PV) almost tripled over the past five years, increasing from 138.9 GW in 2013 to 401.5 GW in 2017.<sup>14,15</sup> With rapid technological advances and cost declines, global installed capacity for solar PV is projected by 2040 to overtake that for all other forms of energy apart from natural gas.<sup>16</sup> Quantitative targets in the National Determined Contributions (NDCs) of the BRI countries would require a commitment in solar power of \$256 billion by 2030, accounting for 55% of total regional renewable investment.<sup>4</sup> Up to 2018, the cumulative investment of solar power in the BRI countries reached \$9.8 billion (see [Table S16](#)), and brought evident economic and environmental benefits.<sup>17,18</sup> Understanding the potential and spatial-temporal distribution of solar power will play a central role in regional planning and policy formation for the development of renewable and zero-carbon energy resources in the BRI region. In addition, a comprehensive analysis of solar power potential can help identify a practical basis for clean energy cooperation within the BRI framework.

A large body of literature has examined the potential of PV solar power on the scale of individual countries, of regions, and of the world as a whole, mostly adopting Geographical Information System (GIS) based multicriteria methods. Hoogwijk pioneered the assessment of the potential for electricity from solar PV on a global scale.<sup>19</sup> More recent studies on the potential for solar PV power emphasized regions, for example, West Africa, the Association of Southeast Asian Nations (ASEAN), and the European Union<sup>20–22</sup>; countries such as Russia, Bangladesh, Pakistan, Oman, China, Iran, and Tanzania<sup>23–29</sup>; or a single city.<sup>30</sup> Studies addressing the assessment of solar power potential tended to identify individual technical factors, such as analysis of land suitability and site selection criteria<sup>29,31–33</sup>; optimization of tilt and orientation of panels to make best use of solar radiation<sup>34–39</sup>; evaluation of the impact of temperature<sup>40</sup>; models of performance under shading conditions,<sup>41,42</sup> quantification of the degradation and performance ratio of solar panels,<sup>43,44</sup> etc. Little research has been devoted to an integrated approach with comprehensive consideration of all of these parameters and their application in modeling the potential of solar PV in the BRI region with high spatial and temporal resolution. The integrated software System Advisor Model (SAM) was developed to provide hourly output information to facilitate specific site selection and to quantify factors influencing investment decision making.<sup>45</sup> However, its application is limited to individual projects and unsuitable for comprehensive analysis from a regional perspective.

<sup>1</sup>School of Environment, State Key Joint Laboratory of Environment Simulation and Pollution Control, Tsinghua University, Beijing, China

<sup>2</sup>Civil and Environmental Engineering, Stanford University, Palo Alto, CA, USA

<sup>3</sup>Institute of Geographic Sciences and Natural Resources Research, Chinese Academy of Sciences, Beijing, China

<sup>4</sup>Harvard John A. Paulson School of Engineering and Applied Sciences, Harvard University, Cambridge, MA, USA

<sup>5</sup>Schwarzman College, Tsinghua University, Beijing, China

<sup>6</sup>Institute of Biological and Environmental Sciences, School of the Biological Sciences, University of Aberdeen, Aberdeen, UK

<sup>7</sup>Department of Earth and Planetary Sciences, Harvard University, Cambridge, MA, USA

<sup>8</sup>These authors contributed equally

<sup>9</sup>Lead Contact

\*Correspondence: [xilu@tsinghua.edu.cn](mailto:xilu@tsinghua.edu.cn) (X.L.), [mbm@seas.harvard.edu](mailto:mbm@seas.harvard.edu) (M.B.M.)

<https://doi.org/10.1016/j.joule.2019.06.006>

In the present study, we developed an integrated approach for solar resource assessment with a focus particularly on evaluating the technical potential for utility-scale solar power in 66 countries across the BRI region. The methodological contribution of the present analysis consists mainly of the following three features. First, power outputs were computed on an hourly basis and aggregated subsequently to evaluate annual electricity generation. This approach not only increases the accuracy of the evaluation of potentials but enables also the temporal variation of solar power to be considered in planning design. Second, spatial variations of factors that will influence electricity generation at real solar farms were modeled using a consistent and comprehensive framework, including consideration of tilt angles, packing density, sun shading, temperature, and system-impacting factors. Finally, solar radiation data with high spatial resolution ( $0.25^\circ$  latitude by  $0.3125^\circ$  longitude) were adopted from Version 5 of the Goddard Earth Observing System Forward Processing (GEOS-5 FP) of the Data Assimilation System (DAS), a resource widely used and validated in studies of atmospheric chemistry that combines a suite of observations, including data from satellites, radiosondes, aircraft, dropsondes, surface ships, and buoys.<sup>46</sup> The practical significance of this approach is reflected in the following dimensions. The study offers a comprehensive description of the technical potential and key parameters for solar PV in the BRI region, a product that can inform future national and regional planning and policy making. The spatial and temporal differences in the distribution and the mismatch between potential production and consumption revealed in the study highlights two important opportunities for clean energy cooperation within the BRI framework. One involves technology transfer among the BRI countries to prioritize exploitation of regions with the best-quality resources for solar power. The other builds on proposals in prior literature for global and regional grid interconnection.<sup>47–49</sup> This last option allows for better matching of demand and supply for solar-generated electricity over the entire region, which in turn can help optimize accommodation of solar power variability.

## RESULTS

### Technical Potential

Annual potential for electricity generation from solar PV power primarily depends on site suitability and resource availability. Site suitability here refers to the availability of large expanses of gently sloping or flat vacant land within constraints of land use type, as well as the exclusion of areas below the feasible limit for economic and technical exploitation of the available annual solar radiation flux (see [Experimental Procedures](#) for details). Resource availability refers to the ability to convert solar energy to electricity with feasible PV tilt, spacing, and orientation settings. The resource availability is adjusted further to account for the spatial influences of temperature and shading. As illustrated in [Figure 1A](#), the total technically feasible solar electricity potential for the BRI countries is as great as 448.9 PWh, equal to 41.3 times the total regional demand for electricity in these countries in 2016. Tapping as little as 3.7 % of the total potential could satisfy the 2030 demand for electricity for the entire region.<sup>50,51</sup> Four countries in the BRI region, namely China, India, Iran, and Saudi Arabia, are listed among the top ten CO<sub>2</sub> emitters in the world and were responsible for 13.2 billion tons of CO<sub>2</sub> emissions or 39.4% of the global total in 2017 (see [Table S4](#)).<sup>52</sup> These countries are estimated to have a solar potential as high as 238.2 PWh, 53.1% of the total for the BRI region. If 30% of the electricity demand in these countries were supplied by solar power, approximately 2.4 billion tons CO<sub>2</sub> could be saved, equivalent to a reduction in global carbon emissions of 7.2%.<sup>53</sup> Countries in the BRI region without current full electricity access also have abundant solar power resources. For example, Yemen, the country in West Asia with the lowest



or by 41.4 PWh for the region (see [Table S11](#)). High ambient air temperature and strong solar insolation leads to elevated panel temperatures, reducing power conversion efficiency and negatively impacting total potential (see [Experimental Procedures](#)). Normally, high latitudes are less susceptible to these negative influences, while temperatures may have a significant negative effect on solar power output in low-latitude areas. For example, the impact of temperature would cause the potential for the Central and Eastern European region and for the Commonwealth of Independent States (CIS) to decrease by 6.0% and 4.4% respectively, compared with a 12.7% decrease in West Asia. If temperature were not considered, the solar potential for the top ten countries would be overestimated by 9.2% on average. This highlights the significance of considering temperature-induced loss of power generation in project planning and site selection. Advance estimates of the impact of temperature can aid in avoiding overly optimistic economic assessments of solar PV deployments, thus reducing investment risk.

The potential capacity for solar power in the BRI region is summarized on a country-by-country basis in [Figure 1B](#), indicating the upper boundary for economically feasible investments in solar PV for individual countries. The total potential capacity for the BRI region is estimated at 265.9 TW, more than 600 times greater than the installed capacity of solar PV globally in 2017. Deployment of 7.8 TW of the most favorable solar power resources in the BRI region could provide a source of electricity equivalent to the total demand projected for the region in 2030. This would require a capital investment of 11.2 trillion 2017 USD.<sup>55</sup> The land area needed for this commitment is as little as 88,426 km<sup>2</sup>, approximately 0.9% of the land area of China.

The distribution of the potential capacity exhibits a similar spatial pattern to the potential of electricity generation, as the latter also varies spatially with land suitability and latitude. The installation density of solar PV panels decreases as the latitude increases because the lower angle of solar incidence in high-latitude regions requires large tilt angles for PV panels to maximize the annual generation of electricity. This in turn requires significant spacing between panel footprints to minimize impacts of inter-panel shading (see [Experimental Procedures](#) for details), resulting in low installed capacity per unit land area. In addition, large areas at high latitudes were excluded because those regions experience more slanted sunlight and a larger fraction of the solar radiation available there tends to lie below the threshold of 1,400 kWh/(m<sup>2</sup>·a) assumed as the lowest boundary for economically justifiable exploitation. As a result, countries located at latitudes higher than 50 degrees, including Russia and some Eastern European countries, have very low potential for solar power in terms of both installed capacity and electricity generation. Fortunately, many of those high-latitude countries enjoy abundant wind power resources, an alternative source of low-carbon energy to replace fossil fuels.<sup>56</sup> For example, the onshore potential for wind power in Russia is estimated to be as high as 120 PWh in contrast to a solar potential of only 3.2 PWh.<sup>56</sup>

### Geographical Distribution of Capacity Factor

We further quantified the annual average capacity factor (CF) for solar PV power in the BRI region, with results for their geographical distribution illustrated in [Figure 2](#). Annual CF, defined by the ratio of annual electricity generated by a solar installation relative to the realization of its full nameplate capacity over the same time period, provides an important measure of the economic attractiveness of capital investment in solar farms. For deployment of solar farms in different locations with equal capacity, a higher CF will lead to greater electricity yields and thus more favorable

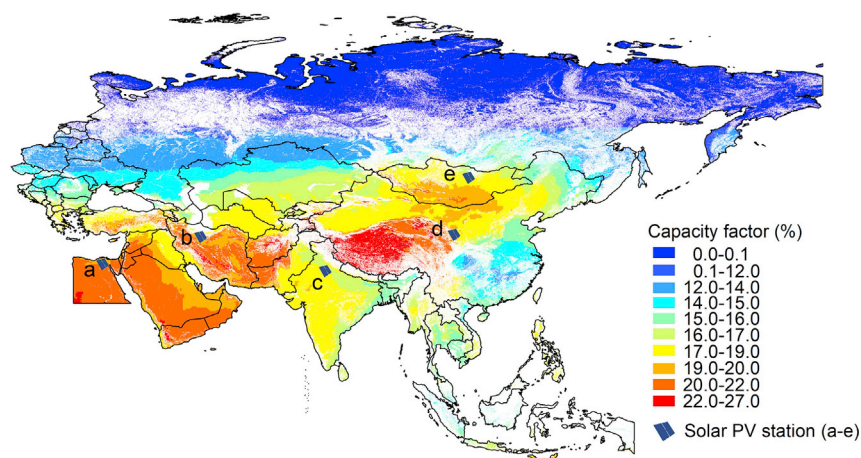


**Figure 2. Capacity Factor Distribution across the BRI Region**

Annual average capacity factor distributions for the BRI countries defined according to the color scale included in the figure. White denotes locations unsuitable for deployment of utility-scale solar PV due to constraints of land use type and/or slope. Dots (a–e) indicate the five hypothetical utility-scale solar stations located near the capital cities of Egypt, Iran, India, Mongolia, and the Gansu Province of China. The solar output profile of the five stations will be used in [Opportunities of Future Grid Interconnection](#) to illustrate the benefits of regional grid interconnection.

returns on potential investments. The value of CF can be used to infer the number of utilization hours (UH), a term widely used in the solar power industry to judge the performance of a solar farm. The corresponding values for UH, equal to CF multiplied by the hours of a year, are presented in [Figure S6](#).

The distribution of CF is driven mainly by the available flux of solar insolation and by PV model parameters, with minor influences from other factors, including temperature, shading, and others. In this sense, CF also defines the resource quality of technically available solar power. As illustrated in red in [Figure 2](#), the CF of the Qinghai-Tibet Plateau reaches as high as 27%, the highest for the entire region. This reflects the high altitude of the region. However, to fully exploit the high available efficiency, supporting grid facilities would be needed to transmit the generated power to load centers. Considering estimates for transmission costs in addition to the difficulty of construction in this environment, this potential is unlikely to be utilized in the near term. High CF is found also for countries in West Asia. Countries such as Yemen, Oman, Saudi Arabia, and Egypt are in low-latitude regions with large land areas of desert benefitting from abundant solar radiation.

[Figure 3A](#) indicates the distribution of solar potential per unit CF and the colors differentiate sources of solar power from individual subareas within the BRI region (see [Table S1](#) and [Figure S1](#) for the countries' classification by subarea). The electricity that could be generated potentially for the entire BRI region is displayed as a function of an assumed CF cutoff applied to potential solar farms in [Figure 3B](#). The results suggest that the total electricity consumption projected for 2030 in the entire BRI region could be supplied by solar PV power while restricting deployment of solar farms to regions where they would be expected to operate with CFs greater than 23.2% (where the blue line crosses the curve in [Figure 3B](#)). The total demand for electricity in 2030 could be satisfied by solar PV power generated in the region if the CF cutoff was reduced to 21.9%.<sup>57</sup> To put this in context, solar PV farms in China had an average CF of 12.9% in 2015.<sup>58</sup> As indicated in [Figure 3B](#), regions with the highest CF are located in South Asia and East Asia, reflecting mainly the favorable solar

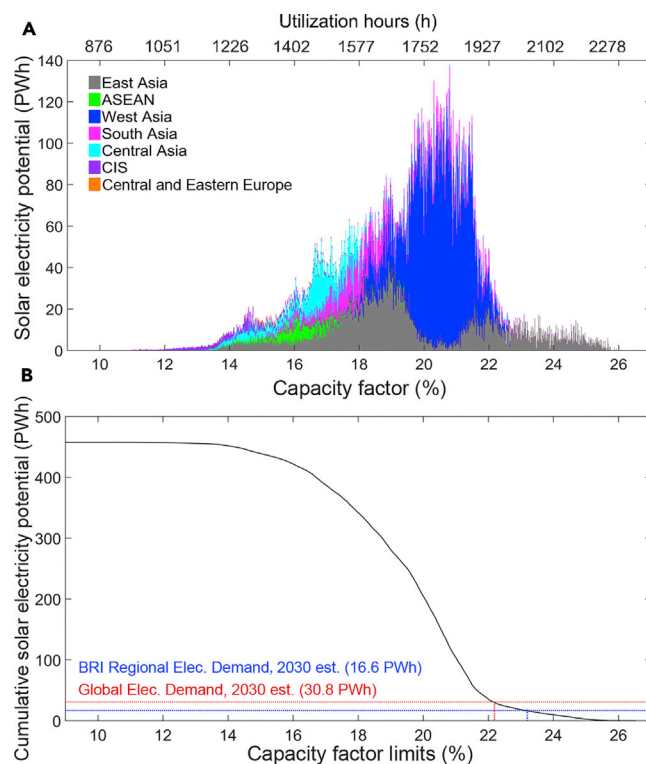


**Figure 3. Relationships between Solar Potential and Capacity Factor**

(A and B) Distribution of annual solar potential by capacity factor (A) and curve of cumulative potential as a function of capacity factor limits (B). The bar height in panel A indicates solar potential from seven subareas by capacity factor. The color composition of each bar represents the subarea contribution of potential for solar electricity. Refer to [Figure S1](#) in the [Supplemental Information](#) for detailed information of the subareas.

radiation in the Qinghai-Tibet Plateau, as indicated in the right-most part of the gray and pink area. The lowest CF maxima are observed in the CIS countries, indicated in purple. Only 16.4% of the potential for the CIS could be realized at sites where CF exceeds 16.0%, which is illustrative of the poor solar radiation conditions for these countries.

West Asia, indicated in blue, enjoys relatively high CF with values ranging from 15.4% to 22.6%. The high marginal solar potential in this CF interval suggests that significant quantities of electricity could be generated potentially also by the deployment of solar farms in West Asia. In fact, the estimated potential for West Asian countries amounts to as high as 208.7 PWh, accounting for 46.5% of the regional total. Dust accumulation on the PV panels may be a concerning issue that could lower the CF of the solar farms in this region, as it may cause physical damages on panels, attenuate the incoming solar radiation, increase surface temperature, and degrade therefore the overall efficiency for power generation.<sup>59</sup> A 10% decrease of annual electricity yield is observed for panels with no cleaning compared with monthly cleaning in the Kingdom of Bahrain.<sup>60</sup> However, the scarcity of water poses a significant challenge for the water-cleaning of panels deployed in the desert nations of this region. Fortunately, self-cleaning methods with little water use, such as electrostatic methods, air-blowing mechanical methods, and coating methods, are being developed, offering a promising application to address these challenges.<sup>61,62</sup>

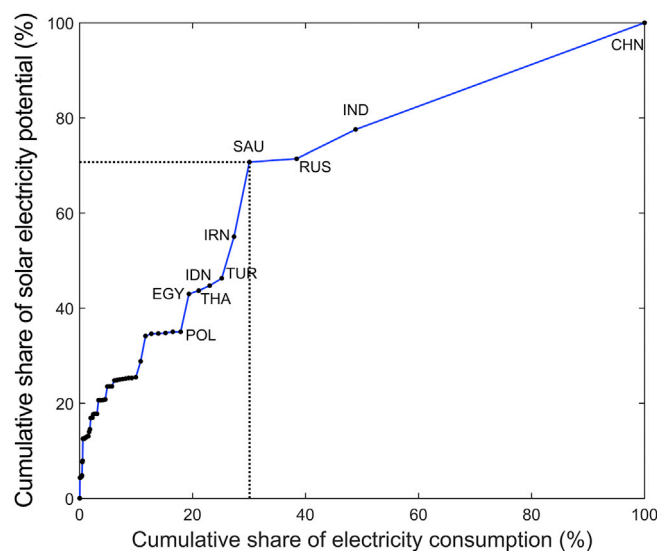


**Figure 4. Lorenz Curve of Solar Potential versus Electricity Consumption**

The dashed lines indicate that 63 out of 66 countries are endowed with 70.7% of the regional total potential of solar electricity but consume 30.1% of regional electricity.

## DISCUSSION

### Future Collaboration on Solar PV

The technical potential is distributed unevenly geographically across the BRI region. The countries within West and East Asia enjoy the highest technical potentials, with regional totals of 207.7 and 122.0 PWh, respectively, accounting together for 73.4% of the total BRI solar potential (see Table S10). In contrast, the potentials of the CIS and Central and East European regions amount to only 4.7 and 1.5 PWh, respectively. The mismatch between solar potentials and domestic electricity demand is reflected by the Lorenz curve in Figure 4. In the BRI region, 63 out of 66 total countries together make up only 30.1% of electricity consumption but could produce as much as 70.7% of the total regional solar potential. This identifies an urgent opportunity for cooperation in transfer technology and experiences under the BRI umbrella, motivated by green incentives: countries rich in solar resources can leapfrog with cost-effective means to utilize their locally abundant solar resources to meet shortages in supplies of electricity elsewhere by exporting surpluses through international markets. Full access to electricity has not been achieved yet in at least 13 of the countries in the BRI region considered here (see Table S2). The potential for solar PV in these power-short countries exceeds their individual demands for electricity by factors ranging from 9 to 5,270. The know-how for constructing and operating solar farms is well established in global leading markets, including China, the US, Japan, Germany, Italy, and India and could be transferred readily to the BRI countries to facilitate development of their available solar resources.<sup>63</sup>

Research by the International Renewable Energy Agency (IRENA) shows that the global average levelized cost of electricity (LCOE) for utility-scale solar PV has dropped from \$0.4/kWh in 2010 to \$0.1/kWh in 2017. The cost is projected to decline to \$0.06/kWh by 2020, even lower on some occasions than fossil fuel-fired electricity.<sup>64</sup> The trend in declining cost is expected to prompt significant large-scale deployment of solar facilities and reduce barriers to solar energy cooperation in the BRI region. With the continuous growth of solar power stations, the impact of scale economies

and breakthroughs in solar conversion efficiency are expected to further reduce the LCOE of solar power, potentially making PV competitive with other technologies (see [Tables S13](#) and [S14](#)). The virtuous cycle of decreasing solar unit costs and increasing installation scale is likely to prompt uptake in solar energy infrastructure that may open new opportunities for regional cooperation to take advantage of the BRI. Multilateral cooperation in the solar PV area will be facilitated also by prioritized investment and financial support offered by the BRI-financing institutions, such as the Asian Infrastructure Investment Bank (AIIB), the Eurasian Development Bank (EDB), Silk Road Fund, and the Asian Development Bank (ADB).<sup>65</sup>

Despite the promising future, efforts are needed to clear barriers to accelerate the penetration of solar power into the BRI regions. First, the lack of economic competitiveness for solar relative to other resources continues to be an obstacle in some BRI countries. Subsidy policies of these BRI countries are either absent or not persistent, which negatively impacts the long-term revenue expectations of the project increasing the investment risk. In addition, with little experience on supply and service chains locally, the high operation and maintenance (O&M) cost keeps the LCOE of solar high. Besides, the decentralized nature of solar power places higher demand on land use compared with traditional power sources. A more consistent subsidy framework combined with tax and/or loan assistance will help drive down the cost of solar and increase the competitiveness. Second, institutional barriers may also inhibit the transnational investment in solar energy because of the diverse and unstable local standards, laws, and regulations. Strengthening communication at the government, industry, and enterprise levels and establishing a standard cooperation framework will facilitate solar energy international cooperation and reduce the investment risks. Third, the relatively poor condition of electric grid systems may inhibit integration of variable sources such as solar power into the grid especially in regions without electricity. Even for countries such as Thailand and Vietnam, where solar is commercially competitive, their national grids are challenged to adopt solar into the power system because of insufficient regulatory capacity.<sup>66</sup> The regional grid interconnection discussed in the following section provides one option to reduce the impact of the variability of solar power.

### Opportunities of Future Grid Interconnection

The imbalanced spatial distribution of technical potentials among subareas suggests an opportunity for export of solar power from high-resource to high-demand countries through regional interconnection of local electricity grids. The overall cost-effectiveness of solar investments in the BRI region could be enhanced by using a regionally interconnected power grid taking advantage of the large range of time zones and weather conditions across the BRI countries. Here we consider an interconnection of five hypothetical solar stations along the BRI economic corridor, located near the capital cities of Egypt, Iran, India, and Mongolia, and Gansu Province in China (see [Table S12](#) for detailed geographic information). Each station is assumed to produce solar power sufficient to meet 30% of the electricity load for its associated city ([Figures 5A](#) and [5B](#)). The spatial complementary effect of transmitting solar power through an interconnected grid and aggregating loads of the five cities will greatly reduce diurnal variations of both supply and demand. In addition, the peak-valley difference of normalized net load (defined as total load minus solar generation) for the interconnected system would be 21.6% lower than the mean level for the five isolated systems ([Figure 5C](#)). The gentler incline of the normalized net load curve when systems are interconnected also enables a smoother dispatch of power over the network. [Figure 5D](#) compares the normalized hour-to-hour variation (ramp rate) over a day for individual systems versus the hypothesized

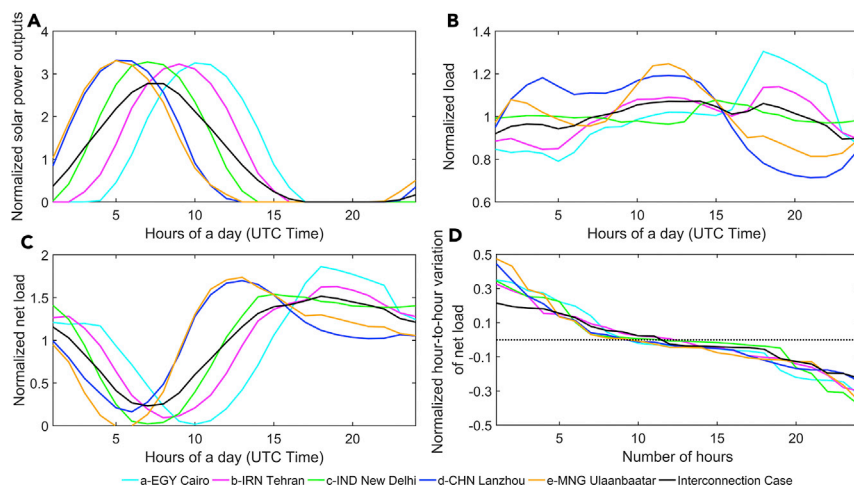


**Figure 5. Smoothing Effect on Hourly Loads and Solar Power Outputs from Electric Grid Interconnection of Five Representative Cities across the BRI Region**

Diurnal variation of annually averaged solar supply from five isolated solar stations (indicated in Figure 2) near Cairo, Egypt, Tehran, Iran, New Delhi, India, Lanzhou, China, and Ulaanbaatar, Mongolia to meet 30% of electricity load of individual cities as compared with an interconnection of above solar stations to meet 30% the aggregated load (A); the same as A but for daily electricity demand profile (B); the same as A but for the net electric load of the five cities and the aggregated demand profile (C); the hour-to-hour variation (or ramp rate) of net load reordered from high to low (D). Curves in Figures 5A–5C are normalized respectively as ratios of the real values to their mean, and Figure 5D is normalized by the mean values of net load expressed in Figure 5C.

interconnected system ordered from high to low. The highest required ramp rate would be reduced by 44.6% for the interconnected system compared to the average for the five isolated systems (Figure 5D). This means that the need for fast-ramping capacity from fossil-fuel generators to compensate for the variability of solar power will be greatly reduced. Although grid interconnection cannot fully resolve the challenges posed by the inherent intermittency of solar PV power (Figures 5C and 5D), its advantage will be significant when multiple renewable sources, including solar, wind, and hydro are complementarily deployed at more locations, to advance the objective of a carbon-free power system for the BRI region.<sup>67</sup>

It is estimated by the Global Energy Interconnection Development and Cooperation Organization (GEIDCO) that the installed capacity of global clean energy could reach 53 TW in 2030 through global energy interconnection with ultra-high voltage (UHV) transmission lines as the backbone.<sup>68</sup> For many countries along the BRI, energy interconnection can be realized by upgrading and expanding existing local interconnected grids rather than by creating new infrastructure. This may allow for easier access, lower costs, and reduced environmental impacts of interconnection infrastructure, as demonstrated in Supplemental Information 15, a case of enabling Kazakhstan access to hydro-power via upgrading the existing Central Asian Unified Power System. Mutual trust among countries, consensus to combat climate change, the maturity of the international electricity trading market, and technological progress in UHV grid and smart grid are all prerequisites to realize energy interconnection in BRI. In addition, transmission loss, noise, land use change, and electromagnetic fields of grid infrastructure need to be further investigated to minimize life cycle environmental impacts.<sup>69–71</sup>

Currently, over 55% of global greenhouse gas (GHG) emissions originate in the BRI region,<sup>72</sup> and this number is expected to rise above 65% by 2030 in the “business as

**Table 1. Setting of Parameters in Three Scenarios**

Setting of Parameters		Conservative Scenario	Moderate Scenario	Liberal Scenario
Suitability Factor of Land Use (%)	All forest	0	0	0
	Closed shrublands, woody savannas	3	5	7
	Grasslands, open shrublands, savannas	15	20	25
	Barren or sparsely vegetated	15	20	25
	Croplands, cropland/natural vegetation mosaic	0	2	4
	Urban and built-up	3	5	7
	Water bodies, permanent wetlands, snow, and ice	0	0	0
Slope (%)	<3	<5	<7	
Solar Radiation (kWh/(m <sup>2</sup> ·a))	>1,400	>1,400	>1,400	

usual" scenario.<sup>73</sup> The growth will be driven not only by large emitters such as China, but also by a range of other countries undergoing rapid scale-up of electrical capacity to power economic growth. Supporting future economic growth in the BRI region with fossil-based energy will make it more difficult to limit future global warming to the limits defined in the Paris Agreement, given that human activity is responsible already for an increase in global average surface temperature of close to 1°C with respect to pre-industrial levels. "Rapid and far-reaching" transitions in energy will be necessary to reduce the risk of long-lasting and irreversible changes.<sup>74</sup> Opportunities are present to constructively enhance the BRI region's fast-growing power sector. As discussed in this study, locally available solar power provides an opportunity for the BRI countries to leapfrog from their carbon-intensive trajectories to low-carbon futures contributing to the GHG control imperatives outlined in Paris.

## EXPERIMENTAL PROCEDURES

### Natural Constraints and Model Configuration

#### Natural Constraints

This study used slope, land use type, and solar radiation as criteria to identify areas suitable for solar farm development. The study includes three sets of parameters in three scenarios: a conservative scenario, a moderate scenario, and a liberal scenario (Table 1). The results and analysis in the main text are based on the moderate scenario. The potential by country under conservative and liberal scenarios are summarized in Tables S8 and S9, and the heterogeneous potential sensitivity among different BRI countries is described in Supplemental Information 10. PV solar farms are best located in flat and open areas with gentle slopes accommodating construction constraints and security considerations. In this study, the maximum permissible slope was set at 5% in the moderate scenario. Slope data were derived from the Shuttle Radar Topography Mission (SRTM) Global Enhanced Slope Database with a spatial resolution of 1 arc-second (approximately 30 meters).<sup>75</sup> Suitability factors were selected according to land use types with higher values allocated to land areas with sparse vegetation and low ecological productivity.<sup>31</sup> The MODIS MCD12Q1 Type 1 data<sup>76</sup> were used to filter unsuitable land areas from this analysis, including forests, water bodies, permanent wetlands, and snow and ice environments. Those areas were excluded by assigning 0% as their suitability factors. For exploitable areas, suitability factors ranging from 2% to 20% were assigned to each land use type in the moderate scenario (Table 1). The minimum solar radiation required for exploitable land areas was set at 1400 kWh/(m<sup>2</sup>·a) in all three scenarios, the threshold values for

acceptable solar resource recommended by the China Meteorological Administration<sup>13</sup> in its Solar Energy Resources Evaluation Methods.

### Solar PV Model

The technology of PV panels assumed in this study is a type of polysilicon modules, which had a global market share of around 70% in 2016.<sup>77</sup> Currently, the conversion efficiency of multi-Si modules in commercial applications<sup>78</sup> is between 14% and 16%, having reached 19.9%<sup>77</sup> under laboratory conditions. The PV conversion efficiency of a 265 W module is set at 16.2%, reflecting an industry average. In this study, the fixed-tilt option was assumed over sun-tracking technologies. Although higher solar power output could be achieved in theory by fully tracking the sun with two-axis systems,<sup>34</sup> fixed-tilt systems are more widely adopted because they are cheaper, simpler, and have lower maintenance requirements.<sup>79</sup>

Under a fixed-tilt system, there is an optimum tilt, azimuth angle (east-west orientation), and spacing that can maximize incoming solar radiation and optimize the sizing of a solar PV farm.<sup>80</sup> Previous studies mainly used latitudes or linear fits of latitude as rules of thumb to roughly predict optimal solar tilt.<sup>81,82</sup> However, heavy cloud cover and haze that exist in many high-latitude countries and regions may cause significant divergence in optimal tilt estimations. Jacobson et al. proposed a 3<sup>rd</sup>-order polynomial fit between optimal tilt and latitude. The optimal tilt data used were derived from the “PV-Watts” program of NREL covering all countries, with one to four representative locations in each country. This method proved to be better than linear fits, especially for latitudes above 40° N.<sup>83</sup> The polynomial fit method used in this study, following the study by Jacobson et al., is as follows (see Table S6 for nomenclature):

$$\Sigma_d = \begin{cases} 1.3793 + \theta(1.2011 + \theta(-0.014404 + \theta * 0.000080509)) & (R=0.96, \text{North Hemisphere}) \\ -0.41657 + \theta(1.4216 + \theta(0.024051 + \theta * 0.00021828)) & (R=0.97, \text{South Hemisphere}) \end{cases}$$

(Equation 4.1)

where  $\Sigma_d$  is tilt in degrees and  $\theta$  is latitude in degrees (see Figure S2). An array of panels is set to face the equator (zero as the azimuth angle) in order to make full use of incoming solar radiation (see Figure S3).<sup>84</sup>

In determining the spacing between footprints of neighboring PV panels, the goal is to eliminate shade on the photovoltaic panels for most of the daytime throughout the year. The altitude angle of the sun is lowest at the winter solstice in the northern hemisphere, when shading is most likely to occur and when largest spacing is required. Thus, the necessary panel spacing during the year is determined using the solar altitude angle at 3 PM at the winter solstice,<sup>85</sup> as expressed by:

$$D = L \cos \Sigma + L \frac{\sin \Sigma}{\tan \beta_n} \cos \phi_s \quad (\text{Equation 4.2})$$

where  $D$  is the panel spacing between neighboring panel footprints;  $L$  is panel length;  $\Sigma$  represents tilt in radians; and  $\beta_n$  and  $\phi_s$  denote solar altitude angle and solar azimuth angle respectively at 3PM at the winter solstice. For the southern hemisphere, the required maximum spacing is calculated similarly, based on the solar position at 3 PM at the southern winter solstice.

### Packing Factor

The packing factor (PF) denotes the effective panel area per square meter of land area and ranges from zero to one, as shown in Equation 4.3. The packing factor is a function of latitude: the higher the latitude, the smaller the PF.

$$PF = \frac{1}{\cos\Sigma + \frac{\sin\Sigma}{\tan\beta_n} \cos\phi_s} \quad (\text{Equation 4.3})$$

The capacity potential (kW) is calculated using Equation 4.4. It is defined as a function of PF multiplied by the power per unit area of the PV panel and the available area of the site:

$$\text{Capacity Potential} = \sum_{j=1}^m \left( \sum_{i=1}^n s_{i,j} \times sf_i \right) \times PF_j \times P_{WP} \div 1000 \quad (\text{Equation 4.4})$$

where  $m$  denotes the total number of pixels in the calculated area;  $n$  denotes the land use suitability category number ( $n = 7$ );  $s_{i,j}$  indicates the area of land use type  $i$  in pixel  $j$  ( $m^2$ );  $sf_i$  is the suitability fraction of land use type  $i$  shown in Table 1; and  $P_{WP}$  represents the power per unit area of the panel ( $P_{WP} = 161.9 \text{ W/m}^2$  in this study).

## Radiation and Other Influential Factors

### Solar Radiation

The solar resource and the potential capacity are two determinants of solar power output. The solar radiation reaching the horizontal surface ( $I_H$ ,  $\text{W/m}^2$ ) can be divided into direct beam ( $I_{BH}$ ) and diffuse radiation ( $I_{DH}$ ). The radiation intercepted by the PV panel ( $I_\Sigma$ ,  $\text{W/m}^2$ ) contains three parts, including direct beam radiation ( $I_{B\Sigma}$ ), diffuse radiation ( $I_{D\Sigma}$ ), and reflected radiation ( $I_{R\Sigma}$ ). In this study, the method introduced by Masters was used to calculate total insolation on a collecting surface as follows<sup>85</sup>:

$$I_{B\Sigma\_coef} = \cot\beta \times \cos\phi \times \sin\Sigma + \cos\Sigma \quad (\text{Equation 4.5})$$

$$I_{D\Sigma\_coef} = \frac{1 + \cos\Sigma}{2} \quad (\text{Equation 4.6})$$

$$I_{R\Sigma\_coef} = \frac{1 - \cos\Sigma}{2} \rho_G \quad (\text{Equation 4.7})$$

$$I_\Sigma = I_{B\Sigma} + I_{D\Sigma} + I_{R\Sigma} = I_{B\Sigma\_coef} \times I_{BH} + I_{D\Sigma\_coef} \times I_{DH} + I_{R\Sigma\_coef} \times I_H \quad (\text{Equation 4.8})$$

where  $I_{B\Sigma\_coef}$ ,  $I_{D\Sigma\_coef}$ ,  $I_{R\Sigma\_coef}$  denote direct beam, diffuse, and reflected conversion coefficients respectively;  $\beta$  and  $\phi$  denote the solar altitude angle and solar azimuth angle respectively; and  $\rho_G$  represents the ground reflectance, with the typical default value for ordinary ground or grass about 0.2. The method is adopted in the study to calculate the incidence of solar radiation on the panels.

### Ambient Temperature

Previous research found that the actual performance of PV panels ranges from 87% to 120% of the theoretical potential because of the influence of ambient temperature.<sup>40</sup> The peak power temperature coefficient is about  $-0.4\%/^\circ\text{C}$  for crystalline-Si modules, meaning that every degree Celsius increase of PV module surface temperature from standard test conditions will result in a 0.4% decrease in power output as compared with the possible maximum. The surface temperature of PV modules and the temperature correction coefficient is calculated in this study on an hourly basis.<sup>85</sup> The solar radiation-surface incident shortwave flux (SWGDN) and temperature at 2 m above the displacement height (T2M) were derived for 2015 and 2016 from the GEOS-5 FP database.<sup>86</sup>

$$T_{cell} = T_{amb} + \left( \frac{NOCT - 20}{0.8} \right) \times I_\Sigma \quad (\text{Equation 4.9})$$

$$TEM_{\text{coef}} = 1 - \delta \times (T_{\text{cell}} - 25) \quad (\text{Equation 4.10})$$

where  $T_{\text{cell}}$  and  $T_{\text{amb}}$  represent the temperature of the PV module surface and the ambient air temperature in degrees Celsius, respectively; NOCT is the normal operating cell temperature, which stands for the cell temperature of a module when the ambient temperature is 20°C, solar irradiation is 0.8 kW/m<sup>2</sup>, and wind speed is 1m/s, the NOCT is 44°C in this analysis;  $I_{\Sigma}$  is the flux of solar insolation on the photovoltaic cell surface in kW/m<sup>2</sup> and  $\delta$  identifies the peak power temperature coefficient (−0.41%/°C).

### Shading

Shading occurs between adjacent arrays at low solar incident angles. A small shading of any part of the panel can severely affect the power output due to series cell connections and hotspots, which will further accelerate the aging of panels and result in increasingly severe malfunctioning.<sup>87</sup> The introduction of bypass diodes in parallel with the cells has reduced the negative impact of shading on power output and the hotspot effect, however, the impact is still nontrivial and the extent of power loss has often been ignored in prior research.<sup>26,40,88</sup> This study first evaluates the shading impacts on solar power potential in a regional analysis. The shading coefficient is calculated as the ratio of shaded area to the total area of the PV panel:

$$SHD_{\text{coef}} = \left( \sin \Sigma \times \cot \beta \times \cos \phi - \frac{\sin \Sigma}{\tan \beta_n} \cos \phi_s \right) \times \frac{\sin \beta_{\text{tmp}}}{\sin(\pi - \beta_{\text{tmp}} - \Sigma)} \quad (\text{Equation 4.11})$$

where  $\beta_{\text{tmp}}$  identifies the projection of the solar altitude angle on the plane parallel to the north-south axis and vertical to the ground, which can be calculated as follows:

$$\beta_{\text{tmp}} = \text{atan}(\tan \beta / \cos \phi_s) \quad (\text{Equation 4.12})$$

This study investigates particularly the shading impact on widely applied PV panels with 60 cells installed in a landscape modality.<sup>42</sup> As illustrated in Figure S4, an individual panel has three subseries circuits, each consisting of 20 cells.<sup>89</sup> The three subseries circuits are paired individually with bypass diodes and then interlinked in a serial configuration. An array consists of four PV panels placed vertically, with each in a landscape modality. Therefore, there will be 12 sets of independent subseries circuits along the tilt direction. If any part of a subseries circuit is shaded, the subseries circuit will be bypassed by the diode and produce no power. Following this rule, the shading coefficient is corrected further using Equation 4.13. The floor function will calculate the largest integer smaller than a given number.

$$SHD_{\text{coef\_cor}} = 1 - \left( \text{floor} \left( SHD_{\text{coef}} \div \frac{1}{12} \right) + 1 \right) \times 1/12 \quad (\text{Equation 4.13})$$

### Power Output Potential

The study computed the power outputs in each hour for individual data grids of GEOS-5 FP database developed by Global Modeling and Assimilation Office (GMAO) of the US National Aeronautics and Space Administration (NASA). The hourly electricity produced per unit land area (W·h/m<sup>2</sup>) is calculated according to:

$$P_h = PF \times P_{\text{WP}} \left[ \frac{I_{\Sigma}}{1000} \right] \left( \frac{\eta}{\eta_{1-\text{sun}}} \right) \times SHD_{\text{coef\_cor}} \times TEM_{\text{coef}} \times SYS_{\text{coef}} \quad (\text{Equation 4.14})$$

where  $\eta$  and  $\eta_{1-\text{sun}}$  identify the photovoltaic conversion efficiencies in the calculated hour and standard test condition (STC, cell temperature of 25°C and an irradiance of 1000 W/m<sup>2</sup> with an air mass 1.5 (AM1.5) spectrum) respectively. Assuming that the

photovoltaic conversion efficiency remains constant when solar radiation changes, the ratio of  $\eta$  to  $\eta_{1-\text{sun}}$  is equal to  $1 I_{\Sigma}$  is the hourly radiation intercepted by the PV panel ( $\text{W}\cdot\text{h}/\text{m}^2$ );  $\text{SYS}_{\text{coef}}$  is the system efficiency factor considering the whole process power loss from power generation to grid connection, 80.56% in this study (see Table S7);  $\text{SHD}_{\text{coef\_cor}}$  and  $\text{TEM}_{\text{coef}}$  denote shading and temperature efficiency factors respectively which were introduced previously.

The impacting factors of temperature, solar radiation and shading effects were evaluated and applied to calculation of the final power outputs on an hourly basis. Differing from potential studies based on daily or monthly data, the approach adopted in this analysis involves an intensive computing load, but allows for more accurate spatial and temporal information quantization, which ultimately results in a more accurate evaluation of the solar power potential at country level and for the BRI region. In addition, the hourly variation obtained from this analysis lays the foundation for further investigation of power system with large-scale penetration of renewable energy. The hourly output data were aggregated then to obtain annual solar potential as shown in Equation 4.15.

Total annual solar electricity potential (kWh) is calculated according to:

$$\text{Generation Potential} = \sum_{k=1}^t \sum_{j=1}^m \left( \sum_{i=1}^n s_{i,j} \times sf_i \right) \times P_{h,k,j} \div 1000 \quad (\text{Equation 4.15})$$

where  $t$  represents hours in the calculated years 2015 and 2016 ( $t = 8,760$ ) and  $P_{h,k,j}$  denotes hourly electricity potential of pixel  $j$  in hour  $k$ . Other variables in the equation are defined above.

The capacity factor (CF) for each analyzed pixel is derived based on an hour-by-hour calculation. CF denotes the ratio of full-load working hours of solar PV panels in a year to the total number of hours in a year. CF is an important indicator of solar power availability taking account of all factors that influence it. Considering the relatively coarse resolution of the GEOS-5 data compared with real project size, there is a risk that we excluded pixels with abundant solar resources from our determination of suitable land area according to solar radiation restrictions based on grid-averaged data. To present a more integral picture of the CF distribution, the restriction of annual average radiation was removed in the discussion of Geographical Distribution of Capacity Factor.

$$\text{CF} = \frac{\text{Full-load working hours in a year(h)}}{\text{Total hours in a year(h)}} \quad (\text{Equation 4.16})$$

### Limitations

Our research developed an integrated evaluation framework for solar power with a comprehensive consideration of technical and physical impacting factors on an hourly basis and applied it to infer the geographical information for solar power potential in the BRI region. Development of solar power in the BRI countries would require further consideration of social and economic constraints, such as incentive policies, as well as land and grid connection costs. In addition, the economic competitiveness of solar PV relative to coal-fired power systems and other renewable sources deserves further investigation for the large-scale application of solar PV in the BRI region.

### SUPPLEMENTAL INFORMATION

Supplemental Information can be found online at <https://doi.org/10.1016/j.joule.2019.06.006>.

## ACKNOWLEDGMENTS

This work was supported by the National Natural Science Foundation of China (71690244 and 71722003), the National Key R&D Program (2016YFC0208901) and Volvo Group in a research project of the Research Center for Green Economy and Sustainable Development, Tsinghua University, and by a grant from the Harvard Global Institute to the Harvard-China Project titled "China 2030/2050: Energy and Environmental Challenges for the Future". K.G.L. was supported by the University of Aberdeen, the Natural Environment Research Council (1806209) United Kingdom, Santander Mobility Award, and the Energy Technology Partnership Post-graduate and Early Career Researcher Grant.

## AUTHOR CONTRIBUTIONS

S.C. and X.L. developed the model and wrote the draft. S.C., X.L., Y.M., K.G.L., Y.D., N.E., Y.W., and J.H. reviewed the draft and offered advice. S.C., X.L., C.P.N., and M.B.M. contributed to designing the research, analyzing the results, and refining the paper.

## DECLARATION OF INTERESTS

The authors declare no competing interests.

Received: January 7, 2019

Revised: April 28, 2019

Accepted: June 4, 2019

Published: June 27, 2019

## REFERENCES

1. National development and reform commission, Ministry of Foreign Affairs, and Ministry of Commerce of the People's Republic of China (2015). Vision and actions on jointly building silk road economic belt and 21st-century maritime silk road. [https://reconasia-production.s3.amazonaws.com/media/filer\\_public/e0/22/e0228017-7463-46fc-9094-0465a6f1ca23/vision\\_and\\_actions\\_on\\_jointly\\_building\\_silk\\_road\\_economic\\_belt\\_and\\_21st-century\\_maritime\\_silk\\_road.pdf](https://reconasia-production.s3.amazonaws.com/media/filer_public/e0/22/e0228017-7463-46fc-9094-0465a6f1ca23/vision_and_actions_on_jointly_building_silk_road_economic_belt_and_21st-century_maritime_silk_road.pdf).
2. The Belt and Road Portal (2018). International cooperation countries. <https://eng.yidaiyilu.gov.cn/gbjj.htm>.
3. Shuai, J., Chen, C.-f., Cheng, J., Leng, Z., and Wang, Z. (2018). Are china's solar PV products competitive in the context of the Belt and Road Initiative? *Energy Policy* 120, 559–568.
4. World Resources Institute (2018). Moving the green Belt and Road initiative: from words to actions. <https://www.bu.edu/gdp/files/2018/11/GDP-and-WRI-BRI-MovingtheGreenbelt.pdf>.
5. World Bank (2017). GDP growth (annual %). [https://data.worldbank.org/indicator/ny.gdp.mktp.kd.zg?name\\_desc=false](https://data.worldbank.org/indicator/ny.gdp.mktp.kd.zg?name_desc=false).
6. International Institute for Applied Systems Analysis (2016). SSP scenario database. [http://www.iiasa.ac.at/web/home/research/researchPrograms/Energy/SSP\\_Scenario\\_Database.html](http://www.iiasa.ac.at/web/home/research/researchPrograms/Energy/SSP_Scenario_Database.html).
7. Liu, Y., and Hao, Y. (2018). The dynamic links between CO<sub>2</sub> emissions, energy consumption and economic development in the countries along "the Belt and Road". *Sci. Total Environ.* 645, 674–683.
8. World Bank (2016). Access to electricity (% of population). <https://data.worldbank.org/indicator/EG.ELC.ACCS.ZS>.
9. World Bank (2016). Population, total. <https://data.worldbank.org/indicator/SP.POP.TOTL>.
10. International Energy Agency (2017). Energy access outlook 2017. [https://www.iea.org/publications/freepublications/publication/WEO2017SpecialReport\\_EnergyAccessOutlook.pdf](https://www.iea.org/publications/freepublications/publication/WEO2017SpecialReport_EnergyAccessOutlook.pdf).
11. Hertwich, E.G., Gibon, T., Bouman, E.A., Arvesen, A., Suh, S., Heath, G.A., Bergesen, J.D., Ramirez, A., Vega, M.I., and Shi, L. (2015). Integrated life-cycle assessment of electricity-supply scenarios confirms global environmental benefit of low-carbon technologies. *Proc. Natl. Acad. Sci. U.S.A.* 112, 6277–6282.
12. World Bank (2016). Global horizontal irradiation. <https://globalsolaratlas.info/?m=sg:ghi>.
13. China Meteorological Center (2008). Solar energy resources evaluation methods QX/T 89–2008. <http://cmastd.cmatc.cn/standardView.jsp?id=369>.
14. European Photovoltaic Industry Association (2014). Global market outlook for photovoltaics 2014–2018. <https://resources.solarbusinesshub.com/solar-industry-reports/item/global-market-outlook-for-photovoltaics-2014-2018>.
15. Solar Power Europe (2017). Global market outlook for solar power / 2017–2021. <https://resources.solarbusinesshub.com/images/reports/172.pdf>.
16. International Energy Agency (2018). World energy outlook 2018. <https://www.iea.org/weo2018/>.
17. State Power Investment Corporation Limited (2017). The CPI power engineering company's Malaysian Belt and road market development documentary. [http://www.cpipec.com/zdt/xwx/jctg/201810/t20181017\\_407.html](http://www.cpipec.com/zdt/xwx/jctg/201810/t20181017_407.html).
18. China Solar Thermal Alliance (2019). Jointly promote and build Belt and Road, and elaborate blueprint for solar thermal power station. <http://www.cnste.org/html/jiaodian/2019/0428/4878.html>.
19. Hoogwijk, M.M. (2004). On the global and regional potential of renewable energy sources, Ph.D dissertation (Utrecht University).
20. Yushchenko, A., de Bono, A., Chatenoux, B., Kumar Patel, M., and Ray, N. (2018). GIS-based assessment of photovoltaic (PV) and concentrated solar power (CSP) generation potential in West Africa. *Renew. Sustain. Energy Rev.* 81, 2088–2103.
21. Siala, K., and Stich, J. (2016). Estimation of the PV potential in ASEAN with a high spatial and

- temporal resolution. *Renew. Energy* **88**, 445–456.
22. Perpiña Castillo, C., Batista e Silva, F., and Lavalle, C. (2016). An assessment of the regional potential for solar power generation in EU-28. *Energy Policy* **88**, 86–99.
  23. Ermolenko, B.V., Ermolenko, G.V., Fetisova, Y.A., and Proskuryakova, L.N. (2017). Wind and solar PV technical potentials: measurement methodology and assessments for Russia. *Energy* **137**, 1001–1012.
  24. Alam Hossain Mondal, M., and Sadrul Islam, A.K.M. (2011). Potential and viability of grid-connected solar PV system in Bangladesh. *Renew. Energy* **36**, 1869–1874.
  25. Khalid, A., and Junaidi, H. (2013). Study of economic viability of photovoltaic electric power for Quetta – Pakistan. *Renew. Energy* **50**, 253–258.
  26. He, G., and Kammen, D.M. (2016). Where, when and how much solar is available? A provincial-scale solar resource assessment for China. *Renew. Energy* **85**, 74–82.
  27. Besarati, S.M., Padilla, R.V., Goswami, D.Y., and Stefanakos, E. (2013). The potential of harnessing solar radiation in Iran: Generating solar maps and viability study of PV power plants. *Renew. Energy* **53**, 193–199.
  28. Aly, A., Jensen, S.S., and Pedersen, A.B. (2017). Solar power potential of Tanzania: identifying CSP and PV hot spots through a GIS multicriteria decision making analysis. *Renew. Energy* **113**, 159–175.
  29. Charabi, Y., and Gastli, A. (2011). PV site suitability analysis using GIS-based spatial fuzzy multi-criteria evaluation. *Renew. Energy* **36**, 2554–2561.
  30. Kausika, B.B., Dolla, O., Folkerts, W., Siebenga, B., Hermans, P., and Sark, W.G.J.H.M. (2015). Bottom-up analysis of the solar photovoltaic potential for a city in the Netherlands: a working model for calculating the potential using high resolution LiDAR data. In *Proceedings of the International Conference on Smart Cities and Green ICT Systems (SMARTGREENS)*.
  31. Noorollahi, E., Fadai, D., Akbarpour Shirazi, M., and Ghodsipour, S. (2016). Land suitability analysis for solar farms exploitation using GIS and Fuzzy Analytic Hierarchy Process (FAHP)—A case study of Iran. *Energies* **9**, 643.
  32. Piyatadsananon, P. (2016). Spatial factors consideration in site selection of ground-mounted PV power plants. *Energy Procedia* **100**, 78–85.
  33. Sánchez-Lozano, J.M., Teruel-Solano, J., Soto-Elvira, P.L., and Socorro García-Cascales, M. (2013). Geographical Information Systems (GIS) and Multi-Criteria Decision Making (MCDM) methods for the evaluation of solar farms locations: case study in south-eastern Spain. *Renew. Sustain. Energy Rev.* **24**, 544–556.
  34. Kacira, M., Simsek, M., Babur, Y., and Demirkol, S. (2004). Determining optimum tilt angles and orientations of photovoltaic panels in Sanliurfa, Turkey. *Renew. Energy* **29**, 1265–1275.
  35. Li, D.H.W., and Lam, T.N.T. (2007). Determining the optimum tilt angle and orientation for solar energy collection based on measured solar radiance data. *Int. J. Photoenergy* **2007**, 1–9.
  36. Hartner, M., Ortner, A., Hiesl, A., and Haas, R. (2015). East to west – the optimal tilt angle and orientation of photovoltaic panels from an electricity system perspective. *Appl. Energy* **160**, 94–107.
  37. Kaddoura, T.O., Ramli, M.A.M., and Al-Turki, Y.A. (2016). On the estimation of the optimum tilt angle of PV panel in Saudi Arabia. *Renew. Sustain. Energy Rev.* **65**, 626–634.
  38. Rowlands, I.H., Kemery, B.P., and Beausoleil-Morrison, I. (2011). Optimal solar-PV tilt angle and azimuth: an Ontario (Canada) case-study. *Energy Policy* **39**, 1397–1409.
  39. Guo, M., Zang, H., Gao, S., Chen, T., Xiao, J., Cheng, L., Wei, Z., and Sun, G. (2017). Optimal tilt angle and orientation of photovoltaic modules using HS algorithm in different climates of China. *Appl. Sci.* **7**.
  40. Kawajiri, K., Oozeki, T., and Genchi, Y. (2011). Effect of temperature on PV potential in the world. *Environ. Sci Technol.* **45**, 9030–9035.
  41. Ramli, M.A.M., Twaha, S., Ishaque, K., and Al-Turki, Y.A. (2017). A review on maximum power point tracking for photovoltaic systems with and without shading conditions. *Renew. Sustain. Energy Rev.* **67**, 144–159.
  42. Barreiro, C., Jansson, P.M., Thompson, A., and Schmalzel, J.L. (2011). PV bypass diode performance in landscape and portrait modalities. In the *Proceedings of the 37th IEEE Photovoltaic Specialists Conference*.
  43. Osterwald, C.R., A.A., Rummel, S., and Ottoson, L. (2002). Degradation analysis of weathered crystalline-silicon PV modules. In the *Proceedings of the 29th PV Specialists Conference*.
  44. SMA Solar Technology AG (2016). Technology AG. Performance ratio-quality factor for the PV plant. <http://files.sma.de/dl/7680/Perfratio-TI-en-11.pdf>.
  45. National Renewable Energy Laboratory (2018). System Advisor Model (SAM) general description, 2017 Version 9.5. <https://www.nrel.gov/docs/fy18osti/70414.pdf>.
  46. Global Modeling and Assimilation Office (2017). File specification for GEOS-5 FP (Forward processing). [https://gmao.gsfc.nasa.gov/products/documents/GEOS\\_5\\_FP\\_File\\_SpecificationON4v1\\_1.pdf](https://gmao.gsfc.nasa.gov/products/documents/GEOS_5_FP_File_SpecificationON4v1_1.pdf).
  47. Wu, G.C., Deshmukh, R., Ndhlukula, K., Radojicic, T., Reilly-Moman, J., Phadke, A., Kammen, D.M., and Callaway, D.S. (2017). Strategic siting and regional grid interconnections key to low-carbon futures in African countries. *Proc. Natl. Acad. Sci. U.S.A* **114**, E3004–E3012.
  48. Ahmed, T., Mekhilef, S., Shah, R., Mithulananthan, N., Seyedmahmoudian, M., and Horan, B. (2017). ASEAN power grid: A secure transmission infrastructure for clean and sustainable energy for South-East Asia. *Renew. Sustain. Energy Rev.* **67**, 1420–1435.
  49. Otsuki, T. (2017). Costs and benefits of large-scale deployment of wind turbines and solar PV in Mongolia for international power exports. *Renew. Energy* **108**, 321–335.
  50. CIA World Factbook 2019 (2019). Electricity consumption (kWh) by country. [https://photius.com/rankings/2019/energy/electricity\\_consumption\\_2019\\_1.html](https://photius.com/rankings/2019/energy/electricity_consumption_2019_1.html).
  51. International Energy Agency (2016). World energy outlook 2016. <https://www.iea.org/newsroom/news/2016/november/world-energy-outlook-2016.html>.
  52. British Petroleum (2018). BP statistical review of world energy 2018. <https://www.bp.com/en/global/corporate/energy-economics/statistical-review-of-world-energy.html>.
  53. World Bank (2014). Carbon dioxide emissions from electricity and heat production, total (% of total fuel combustion). <https://data.worldbank.org/indicator/EN.CO2.ETOT.ZS>.
  54. Central Intelligence Agency (2018). Yemen energy data 2018. [https://theodora.com/wfbcurren/yemen/yemen\\_energy.html](https://theodora.com/wfbcurren/yemen/yemen_energy.html).
  55. National Renewable Energy Laboratory (2018). U.S. solar photovoltaic system cost benchmark. <https://www.nrel.gov/docs/fy19osti/72399.pdf>.
  56. Lu, X., McElroy, M.B., and Kiviluoma, J. (2009). Global potential for wind-generated electricity. *Proc. Natl. Acad. Sci. U.S.A* **106**, 10933–10938.
  57. U.S. Energy Information Administration (2016). International energy outlook 2016. [www.eia.gov/forecasts/ieo](http://www.eia.gov/forecasts/ieo).
  58. National Energy Administration (2016). Photovoltaic power generation related statistics. [http://www.nea.gov.cn/2016-02/05/c\\_135076636.htm](http://www.nea.gov.cn/2016-02/05/c_135076636.htm).
  59. Zaihede, F.M., Mekhilef, S., Seyedmahmoudian, M., and Horan, B. (2016). Dust as an unalterable deteriorative factor affecting PV panel's efficiency: why and how. *Renew. Sustain. Energy Rev.* **65**, 1267–1278.
  60. Alnaser, N.W., Al Othman, M.J., Dakhel, A.A., Batarseh, I., Lee, J.K., Najmaii, S., Allothman, A., Al Shawaikh, H., and Alnaser, W.E. (2018). Comparison between performance of man-made and naturally cleaned PV panels in a middle of a desert. *Renew. Sustain. Energy Rev.* **82**, 1048–1055.
  61. Moharram, K.A., Abd-Elhady, M.S., Kandil, H.A., and El-Sherif, H. (2013). Influence of cleaning using water and surfactants on the performance of photovoltaic panels. *Energy Convers. Manag.* **68**, 266–272.
  62. Syafiq, A., Pandey, A.K., Adzman, N.N., and Rahim, N.A. (2018). Advances in approaches and methods for self-cleaning of solar photovoltaic panels. *Sol. Energy* **162**, 597–619.
  63. Wang, C., and Wang, F. (2017). China can lead on climate change. *Science* **357**, 764.
  64. International Renewable Energy Agency (2018). Renewable power generation costs in 2017. [https://www.irena.org/media/Files/IRENA/Agency/Publication/2018/Jan/IRENA\\_2017\\_Power\\_Costs\\_2018.pdf](https://www.irena.org/media/Files/IRENA/Agency/Publication/2018/Jan/IRENA_2017_Power_Costs_2018.pdf).
  65. Asian Infrastructure Investment Bank (2018). Financing Asia's future: 2017 annual report and financials. <https://www.aiib.org/en/news-events/news/2017/annual-report/common/pdf/AIIB-Annual-Report-2017.pdf>.

66. Eyler, B. (2019). Can solar diplomacy green the Belt and Road?. <https://www.chinadialogue.net/article/show/single/en/11037-Can-solar-diplomacy-green-the-Belt-and-Road->.
67. Jacobson, M.Z., Delucchi, M.A., Bauer, Z.A.F., Goodman, S.C., Chapman, W.E., Cameron, M.A., Bozonnat, C., Chobadi, L., Clonts, H.A., Enevoldsen, P., et al. (2017). 100% clean and renewable wind, water, and sunlight all-sector energy roadmaps for 139 countries of the world. *Joule* 1, 108–121.
68. The United Nations framework convention on climate change (2018). Global energy interconnection is crucial for Paris goals. <https://unfccc.int/news/global-energy-interconnection-is-crucial-for-paris-goals>.
69. Jorge, R.S., and Hertwich, E.G. (2013). Environmental evaluation of power transmission in Norway. *Appl. Energy* 101, 513–520.
70. Jorge, R.S., and Hertwich, E.G. (2014). Grid infrastructure for renewable power in Europe: the environmental cost. *Energy* 69, 760–768.
71. Wei, W., Wu, X., Li, J., Jiang, X., Zhang, P., Zhou, S., Zhu, H., Liu, H., Chen, H., Guo, J., et al. (2018). Ultra-high voltage network induced energy cost and carbon emissions. *J. Cleaner Prod.* 178, 276–292.
72. Global Carbon Project (2018). Global budgets for greenhouse gases. <http://www.globalcarbonproject.org/>.
73. The Climate Equity Reference Project (2018). The climate equity reference calculator. <https://calculator.climateequityreference.org/>.
74. Intergovernmental Panel on Climate Change (2018). Summary for policymakers of IPCC special report on global warming of 1.5°C approved by governments. [http://www.ipcc.ch/pdf/session48/pr\\_181008\\_P48\\_spm\\_en.pdf](http://www.ipcc.ch/pdf/session48/pr_181008_P48_spm_en.pdf).
75. U.S. Geological Survey (2015). Shuttle radar topography mission (SRTM). <https://lta.cr.usgs.gov/SRTM>.
76. U.S. Geological Survey (2014). Land cover type yearly L3 global 500m SIN grid. [https://lpdaac.usgs.gov/dataset\\_discovery/modis/modis\\_products\\_table/mcd12q1](https://lpdaac.usgs.gov/dataset_discovery/modis/modis_products_table/mcd12q1).
77. Fraunhofer Institute for Solar Energy Systems, and I.S.E. (2018). Photovoltaics report 2018. <https://www.ise.fraunhofer.de/content/dam/ise/de/documents/publications/studies/Photovoltaics-Report.pdf>.
78. World Energy Council (2016). World energy resources solar 2016. [https://www.worldenergy.org/wp-content/uploads/2017/03/WEResources\\_Solar\\_2016.pdf](https://www.worldenergy.org/wp-content/uploads/2017/03/WEResources_Solar_2016.pdf).
79. International Finance Corporation (2015). Utility-scale solar photovoltaic power plants: a project developer's guide. [https://www.ifc.org/wps/wcm/connect/f05d3e00498e0841bb6fbbe54d141794/IFC+Solar+Report\\_Web+\\_08+05.pdf?MOD=AJPERES](https://www.ifc.org/wps/wcm/connect/f05d3e00498e0841bb6fbbe54d141794/IFC+Solar+Report_Web+_08+05.pdf?MOD=AJPERES).
80. Yadav, A.K., and Chandel, S.S. (2013). Tilt angle optimization to maximize incident solar radiation: a review. *Renew. Sustain. Energy Rev.* 23, 503–513.
81. Chang, T.P. (2009). The Sun's apparent position and the optimal tilt angle of a solar collector in the northern hemisphere. *Sol. Energy* 83, 1274–1284.
82. Talebizadeh, P., Mehrabian, M.A., and Abdolzadeh, M. (2011). Determination of optimum slope angles of solar collectors based on new correlations. *Energy Sources A* 33, 1567–1580.
83. Jacobson, M.Z., and Jadhav, V. (2018). World estimates of PV optimal tilt angles and ratios of sunlight incident upon tilted and tracked PV panels relative to horizontal panels. *Sol. Energy* 169, 55–66.
84. Bas, L. (2011). Calculating your optimal azimuth angle. <https://www.civicsolar.com/support/installer/articles/calculating-your-optimal-azimuth-angle>.
85. Masters, G.M. (2004). Renewable and efficient electric power systems (John Wiley & Sons, Inc.).
86. Lucchesi, R. (2017). File specification for GEOS-5 FP: GMAO Office Note No. 4, [1.1 Version]. [https://gmao.gsfc.nasa.gov/products/documents/GEOS\\_5\\_FP\\_File\\_Specification\\_ON4v1\\_1.pdf](https://gmao.gsfc.nasa.gov/products/documents/GEOS_5_FP_File_Specification_ON4v1_1.pdf).
87. Ahsan, S., Niazi, K.A.K., Khan, H.A., and Yang, Y. (2018). Hotspots and performance evaluation of crystalline-silicon and thin-film photovoltaic modules. *Microelectron. Reliab.* 1014–1018.
88. Anwarzai, M.A., and Nagasaka, K. (2017). Utility-scale implementable potential of wind and solar energies for Afghanistan using GIS multi-criteria decision analysis. *Renew. Sustain. Energy Rev.* 71, 150–160.
89. Trinasolar. (2017). Product details of polysilicon module. [http://static.trinasolar.com/sites/default/files/PS-M-0323%20F%20Datashet\\_Allmax\\_US\\_Sep2017\\_B.pdf](http://static.trinasolar.com/sites/default/files/PS-M-0323%20F%20Datashet_Allmax_US_Sep2017_B.pdf).